

1 **Simulation of ozone-vegetation coupling and feedback in**
2 **China using multiple ozone damage schemes**

3
4
5 Jiachen Cao¹, Xu Yue^{1*}, Mingrui Ma²
6

7 1. Jiangsu Key Laboratory of Atmospheric Environment Monitoring and Pollution
8 Control, Collaborative Innovation Center of Atmospheric Environment and Equipment
9 Technology, School of Environmental Science and Engineering, Nanjing University of
10 Information Science & Technology (NUIST), Nanjing, 210044, China

11 2. State Key Laboratory of Pollution Control and Resource Reuse, School of the
12 Environment, Nanjing University, Nanjing, 210044, China

13
14
15
16 *Corresponding author: Xu Yue

17 email: [yuexu@nuist.edu.cn](mailto:yuxu@nuist.edu.cn)
18
19
20
21
22
23
24

Abstract

As a phytotoxic pollutant, surface ozone (O_3) not only affects plant physiology but also influences meteorological fields and air quality by altering leaf stomatal functions. Previous studies revealed strong feedbacks of O_3 -vegetation coupling in China but with large uncertainties due to the applications of varied O_3 damage schemes and chemistry-vegetation models. In this study, we quantify the O_3 vegetation damage and the consequent feedbacks to surface meteorology and air quality in China by coupling two O_3 damage schemes (S2007 vs. L2013) into a fully coupled regional meteorology-chemistry model. With different schemes and damaging sensitivities, surface O_3 is predicted to decrease summertime gross primary productivity by 5.5%-21.4% and transpiration by 5.4%-23.2% in China, in which the L2013 scheme yields 2.5-4 times of losses relative to the S2007 scheme. The damages to photosynthesis of sunlit leaves are ~ 2.6 times that of shaded leaves in the S2007 scheme but show limited differences in the L2013 scheme. Though with large discrepancies in offline responses, the two schemes yield similar magnitude of feedback to surface meteorology and O_3 air quality. The O_3 -induced damage to transpiration increases national sensible heat by 3.2-6.0 W m^{-2} (8.9% to 16.2%) while reduces latent heat by 3.3-6.4 W m^{-2} (-5.6% to -17.4%), leading to a 0.2-0.51 $^{\circ}C$ increase in surface air temperature and a 2.2-3.9% reduction in relative humidity. Meanwhile, surface O_3 concentrations on average increase by 2.6-4.4 $\mu g m^{-3}$ due to the inhibitions of stomatal uptake and the anomalous enhancement in isoprene emissions, the latter of which is attributed to the surface warming by O_3 -vegetation coupling. Our results highlight the importance of O_3 control in China due to its adverse effects on ecosystem functions, global warming, and O_3 pollution through the O_3 -vegetation coupling.

Keywords: Ozone, vegetation, feedback, meteorology, air quality, regional model

52 **1 Introduction**

53 Surface ozone (O_3) is one of the most enduring air pollutants affecting air quality
54 in China, with detrimental effects on human health and ecosystem functions (Monk et
55 al., 2015). Long-term observations and numerical simulations have shown that O_3
56 affects stomatal conductance (Li et al., 2017), accelerates vegetation aging (Feng et al.,
57 2015), and reduces photosynthesis (Wittig et al., 2007). These negative effects altered
58 carbon allocation (Yue and Unger, 2014; Lombardozzi et al., 2015) and inhibited plant
59 growth (Li et al., 2016), suppressing ecosystem carbon uptake (Ainsworth, 2012).
60 Moreover, these effects have profound implications for global/regional climate and
61 atmospheric environment. Given the significant ecological impacts, a systematic
62 quantification of the O_3 vegetation damage effect in China is of great importance for
63 the better understanding of the side effects of O_3 pollution on both regional carbon
64 uptake and climate change.

65 At present, field experiments on O_3 -induced vegetation damage have been
66 conducted in China but were mostly confined to individual monitoring sites. For
67 instance, Su et al. (2017) conducted experiments on grassland in Inner Mongolia and
68 found that elevated O_3 concentrations resulted in a decrease of approximately 20% in
69 the photosynthetic rate of herbaceous plants. Meta-analysis of tropical, subtropical, and
70 temperate tree species in China found that increased O_3 concentrations reduced net
71 photosynthesis and total biomass of Chinese woody plants by 28% and 14%,
72 respectively (Li et al., 2017). However, most of these experiments were conducted
73 using open-top chambers with artificially controlled O_3 concentrations, rather than
74 actual surface O_3 concentrations, making it difficult to quantitatively estimate the
75 impact of ambient O_3 on vegetation productivity. Furthermore, the spatial coverage of
76 field experiments is limited, which hinders the direct use of observational data for
77 assessing O_3 vegetation damage in different regions of China.

78 Alternatively, numerical models provide a more feasible approach to quantify the
79 O_3 -induced vegetation damage from the regional to global scales. Currently, there are
80 three main parameterizations for the calculation of ozone vegetation damage. Felzer et

81 al. (2004) established an empirical scheme based on the Accumulated Ozone exposure
82 over a Threshold of 40 ppb (AOT40) within the framework of a terrestrial ecosystem
83 model. They further estimated that O₃ pollution in the United States led to a decrease
84 in net primary productivity (NPP) by 2.6% to 6.8% during the period of 1980-1990.
85 However, the AOT40 is related to O₃ concentrations alone and ignores the biological
86 regulations on the O₃ stomatal uptake, leading to inconsistent tendencies between O₃
87 pollution level and plant damage at the drought conditions (Gong et al., 2021). In
88 acknowledge of such deficit, Sitch et al. (2007) proposed a semi-mechanistic scheme
89 calculating O₃ vegetation damage based on the stomatal uptake of O₃ fluxes and the
90 coupling between stomatal conductance and leaf photosynthesis. Yue and Unger (2014)
91 implemented this scheme into the Yale Interactive terrestrial Biosphere (YIBs) model.
92 Taking into account varied O₃ sensitivities of different vegetation types, they estimated
93 that surface O₃ led to reductions of 2-5% in the summer gross primary productivity
94 (GPP) in eastern U.S. from 1998 to 2007. Later, Lombardozzi et al. (2013) conducted
95 a meta-analysis using published chamber data and found different levels of responses
96 to O₃ exposure between stomatal conductance and photosynthesis. They further
97 implemented the independent response relationships into the Community Land Model
98 (CLM) and estimated that current ozone levels led to a reduction in global GPP by 8%-
99 12% (Lombardozzi et al., 2015).

100 The O₃ stress on vegetation physiology can feed back to affect regional climate.
101 Lombardozzi et al. (2015) employed the CLM model and found that current O₃
102 exposure reduced transpiration by 2%-2.4% globally and up to 15% regionally over
103 eastern U.S., Europe, and Southeast Asia, leading to further perturbations in surface
104 energy balance. In U.S., Li et al. (2016) found that the O₃ vegetation damage reduced
105 latent heat (LH) flux, precipitation, and runoff by 10-27 W m⁻², 0.9-1.4 mm d⁻¹, and
106 0.1-0.17 mm d⁻¹, respectively, and increased surface air temperature by 0.6-2.0 °C
107 during the summer of 2007-2012. In China, Zhu et al. (2022) performed simulations
108 and found that the inclusion of O₃-vegetation interaction caused a 5-30 W m⁻² decrease
109 in LH, 0.2-0.8 °C increase in surface air temperature, and 3% reduction in relative

110 humidity during summers of 2014-2017. Recently, Jin et al. (2023) applied a different
111 regional model and estimated that O₃ exposure weakened plant transpiration and altered
112 surface heat flux in China, resulting in significant increase of up to 0.16 °C in maximum
113 daytime temperature and decrease of -0.74% in relative humidity. However, all these
114 previous estimates of O₃-induced feedback to climate were derived using the empirical
115 O₃ damage scheme proposed by Lombardozzi et al. (2013), which assumed fixed
116 damage ratios independent of O₃ dose for some vegetation species and as a result may
117 have biases in the further estimated feedback to climate.

118 The O₃-vegetation coupling also has intricate implications for air quality. On one
119 hand, O₃-vegetation coupling can influence meteorological conditions that affect O₃
120 generation, ultimately influencing the O₃ level (Sadiq et al., 2017). On the other hand,
121 it can also influence biogenic emissions and dry deposition, thereby affecting O₃
122 concentrations (Gong et al., 2020). Sadiq et al. (2017) implemented O₃-vegetation
123 coupling in the Community Earth System Model (CESM) and estimated that surface
124 O₃ concentrations increased 4-6 ppb in Europe, North America, and China due to O₃-
125 vegetation coupling. By using the CLM model with the empirical scheme of
126 Lombardozzi et al. (2013), Zhou et al. (2018) found that O₃-induced damage on leaf
127 area index (LAI) could lead to changes in global O₃ concentrations by -1.8 to +3 ppb
128 in boreal summer. Gong et al., (2020) used the O₃ damage scheme from Sitch et al.
129 (2007) embedded in a global climate-chemistry-carbon coupled model and estimated
130 that O₃-induced stomatal inhibition led to an average surface O₃ increase of 1.2-2.1 ppb
131 in eastern China and 1.0-1.3 ppb in western Europe. Different from the above global
132 simulations with coarse resolutions, regional modeling with fine resolution can reveal
133 more details about O₃-vegetation coupling and feedback to surface O₃ concentrations
134 in China (Zhu et al., 2022; Jin et al., 2023). However, all these regional simulations
135 were carried out using O₃ damage scheme of Lombardozzi et al. (2013), limiting the
136 exploration of model uncertainties due to varied O₃ vegetation damage schemes.

137 In this study, we implemented O₃ vegetation damage schemes from both Sitch et
138 al. (2007) and Lombardozzi et al. (2013) into the widely-used regional meteorology-

139 chemistry model WRF-Chem. We validated the simulated meteorology and O₃
140 concentrations, and performed sensitivity experiments to explore the O₃ damage to GPP
141 and consequent feedbacks to regional climate and air quality in China. Within the same
142 framework, we compared the differences of O₃-vegetation coupling from two schemes
143 and explored the causes for the discrepancies. We aimed to quantify the modeling
144 uncertainties in the up-to-date estimates of O₃ impact on regional carbon fluxes and its
145 feedback to regional climate and air quality in China.

146

147 **2 Method**

148 **2.1 WRF-Chem model**

149 We used WRF-Chem model version 3.9.1 to simulate meteorological fields and
150 O₃ concentration in China. The model includes atmospheric physics and dynamical
151 processes, atmospheric chemistry, and biophysical and biochemical processes (Grell et
152 al., 2005, Skamarock et al., 2008). The model domain is configured with 196×160 grid
153 cells at 27 km horizontal resolution on the Lambert conformal projection, and covers
154 the entire mainland China. In the vertical direction, 28 layers are set extending from
155 surface to 50 hPa. The meteorological initial and boundary conditions were adopted
156 from ERA5 reanalysis produced by the European Centre for Medium-Range Weather
157 Forecasts (ECMWF) at a horizontal resolution of 0.25°×0.25° (Hersbach et al., 2020).
158 The chemical initial and boundary conditions were generated from the Model for Ozone
159 and Related Chemical Tracer version 4 (MOZART-4), which is available at a horizontal
160 resolution of 1.9°×2.5° with 56 vertical layers (Emmons et al., 2010).

161 Anthropogenic emissions are adopted from the 0.25° Multi-resolution Emission
162 Inventory for China (MEIC) and MIX Asian emission inventory for the other regions
163 (available at <http://meicmodel.org>). Biogenic emissions are calculated online using the
164 Model of Emissions of Gases and Aerosols from Nature (Guenther et al., 2006), which
165 considers the impacts of plant types, weather conditions, and leaf area on vegetation
166 emissions. Atmospheric chemistry is simulated using the Carbon Bond Mechanism
167 version Z (CBMZ) (Zaveri and Peters, 1999) gas-phase chemistry module coupled with

168 a four-bin sectional Model for Simulating Aerosol Interactions and Chemistry
 169 (MOSAIC) (Zaveri et al., 2008). The photolysis scheme is based on the Madronich
 170 Fast-TUV photolysis module (Tie et al., 2003). The physical configurations include the
 171 Morrison double-moment microphysics scheme (Morrison et al., 2009), the Grell-3
 172 cumulus scheme (Grell et al., 2002), the Rapid Radiative Transfer Model longwave
 173 radiation scheme (Mlawer et al., 1997), the Goddard short-wave radiation scheme
 174 (Chou and Suarez, 1994), the Yonsei University planetary boundary layer scheme
 175 (Hong et al., 2006), and the revised MM5 (Fifth generation Mesoscale Model) Monin–
 176 Obukhov surface layer scheme.

177

178 **2.2 Noah-MP model**

179 Noah-MP is a land surface model coupled to WRF-Chem with multiple options
 180 for key land-atmosphere interaction processes (Niu et al., 2011). Noah-MP considers
 181 canopy structure with canopy height and crown radius, and depicts leaves with
 182 prescribed dimensions, orientation, density, and radiometric properties. The model
 183 employs a two-stream radiative transfer approach for surface energy and water transfer
 184 processes (Dickinson, 1983). Noah-MP is capable of distinguishing photosynthesis
 185 pathways between C₃ and C₄ plants, and defines vegetation-specific parameters for leaf
 186 photosynthesis and respiration.

187 Noah-MP considers prognostic vegetation growth through the coupling between
 188 photosynthesis and stomatal conductance (Farquhar et al., 1980; Ball et al., 1987). The
 189 photosynthesis rate, A ($\mu\text{molCO}_2 \text{ m}^{-2} \text{ s}^{-1}$), is calculated as one of three limiting factors
 190 as follows:

$$191 \quad A_{tot} = \min(W_c, W_j, W_e)I_{gs} \quad (1)$$

192 where W_c is the RuBisco-limited photosynthesis rate, W_j is the light-limited
 193 photosynthesis rate, and W_e is the export-limited photosynthesis rate. I_{gs} is the
 194 growing season index with values ranging from 0 to 1. Stomatal conductance (g_s) is
 195 computed based on photosynthetic rate as follows:

$$196 \quad g_s = \frac{1}{r_s} = m \frac{A_{net}}{C_s} RH + b \quad (2)$$

197 where b is the minimum stomatal conductance; m is the Ball-Berry slope of the
 198 conductance-photosynthesis relationship; A_{net} is the net photosynthesis by subtracting
 199 dark respiration from A_{tot} ; C_s is the ambient CO₂ concentration at the leaf surface. The
 200 assimilated carbon is allocated to various parts of vegetation (leaf, stem, wood, and root)
 201 and soil carbon pools (fast and slow), which determines the variations of LAI and
 202 canopy height. Plant transpiration rate is then estimated using the dynamic LAI and
 203 stomatal conductance. Noah-MP also distinguishes the photosynthesis of sunlit and
 204 shaded leaves. Sunlit leaves are more limited by CO₂ concentration while shaded leaves
 205 are more constrained by insolation, leading to varied responses to O₃ damage.

206

207 **2.3 Scheme for ozone damage on vegetation**

208 We implemented the O₃ vegetation damage schemes proposed by Sitch et al. (2007)
 209 (thereafter S2007) and Lombardozzi et al. (2013) (thereafter L2013) into the Noah-MP.
 210 In S2007 scheme, the undamaged fraction F for net photosynthesis is dependent on the
 211 sensitivity parameter a_{PFT} and excessive area-based stomatal O₃ flux, which is
 212 calculated as the difference between f_{O_3} and threshold y_{PFT} :

$$213 \quad F = 1 - a_{PFT} \times \max\{f_{O_3} - y_{PFT}, 0\} \quad (3)$$

214 where a_{PFT} and y_{PFT} are specifically determined for individual plant functional types
 215 (PFTs) based on measurements (Table 1). The stomatal O₃ flux f_{O_3} is calculated as

$$216 \quad f_{O_3} = \frac{[O_3]}{r_a + k_{O_3} \cdot r_s} \quad (4)$$

217 where $[O_3]$ is the O₃ concentration at the reference level (nmol m⁻³), r_a is the
 218 aerodynamic and boundary layer resistance between leaf surface and reference level (s
 219 m⁻¹). $k_{O_3} = 1.67$ represents the ratio of leaf resistance for O₃ to that for water vapor. r_s
 220 represents stomatal resistance (s m⁻¹). For S2007 scheme, stomatal conductance is
 221 damaged with the same ratio (1- F) as photosynthesis and further affects O₃ uptake. In
 222 Noah-MP, the f_{O_3} are calculated separately for sunlit and shaded leaves with
 223 corresponding stomatal resistance (Supplementary Text S1).

224 As a comparison, the L2013 scheme applies separate O₃ damaging relationships

225 for photosynthetic rate and stomatal conductance. These independent relationships
226 account for different plant groups and are calculated based on the cumulative uptake of
227 O₃ (CUO) under different levels of chronic O₃ exposure. The leaf-level CUO (mmol m⁻²)
228 ²) is calculated by accumulating stomatal O₃ fluxes of Equation 4 from the start of the
229 growing season to the specific time step with mean LAI > 0.5 (Lombardozzi et al.,
230 2012), when vegetation is most vulnerable to air pollution episodes. O₃ uptake is only
231 accumulated when O₃ flux is above an instantaneous threshold of 0.8 nmol O₃ m⁻² s⁻¹
232 to account for ozone detoxification by vegetation at low O₃ levels (Lombardozzi et al.,
233 2015). We also include a leaf-turnover rate for evergreen plants so that the accumulation
234 of O₃ flux does not last beyond the average foliar lifetime. The O₃ damaging ratios
235 depend on CUO with empirical linear relationships as follows:

$$236 F_{pO_3} = a_p \times CUO + b_p \quad (5)$$

$$237 F_{cO_3} = a_c \times CUO + b_c \quad (6)$$

238 where F_{pO_3} and F_{cO_3} are the ozone damage ratios for photosynthesis and stomatal
239 conductance, respectively. The slopes (a_p for photosynthesis and a_c for stomatal
240 conductance) and intercepts (b_p for photosynthesis and b_c for stomatal conductance) of
241 regression functions are determined based on the meta-analysis of hundreds of
242 measurements (Table 2). The ratios predicted in Equations (5) and (6) are applied to
243 photosynthesis and stomatal conductance, respectively, to account for their independent
244 responses to O₃ damages. In Noah-MP, the F_{pO_3} and F_{cO_3} are calculated separately for
245 sunlit and shaded leaves based on corresponding stomatal resistance (Supplementary
246 Text S1).

247

248 **2.4 Observational data**

249 We validated the simulated meteorology and air pollutants with observations. The
250 meteorological data were downloaded from the National Meteorological Information
251 Center of China Meteorological Administration (CMA Meteorological Data Centre,
252 2022, <http://data.cma.cn/data/detail/dataCode/A.0012.0001.html>). The daily averaged
253 surface pressure (PRES), wind speed at a height of 10 m (WS10), relative humidity
254 (RH) and temperature at a height of 2 m (T2) were collected from 839 ground stations.

255 Hourly surface O₃ concentrations at 1597 sites in China were collected from Chinese
256 National Environmental Monitoring Center (CNEMC, <http://websearch.mep.gov.cn/>).

257

258 **2.5. Simulations**

259 We performed seven experiments to quantify the damaging effects of ambient O₃
260 on GPP and the feedbacks to regional climate and air quality (Table 3). All simulations
261 are conducted from 1st May to 31st August of 2017 with the first month excluded from
262 the analysis as the spin-up. The control simulations (CTRL) excluded the impact of
263 ozone on vegetation. Three offline simulations were performed with the same settings
264 as the CTRL run, except that O₃ vegetation damages were calculated and output without
265 feedback to affect vegetation growth. These offline runs were established using either
266 the S2007 scheme (Offline_SH07 for high sensitivity and Offline_SL07 for low
267 sensitivity) or the L2013 scheme (Offline_L13). As a comparison, three online
268 simulations applied the S2007 scheme (Online_SH07 for high sensitivity and
269 Online_SL07 for low sensitivity) and the L2013 scheme (Online_L13) to estimate the
270 O₃ damages to GPP, which further influenced LAI development, leaf transpiration, and
271 dry deposition. The differences between CTRL and Online runs indicated the responses
272 of surface meteorology and O₃ concentrations to the O₃-induced vegetation damages.

273

274 **3. Results**

275 **3.1 Model evaluations**

276 We compared the simulated summer near-surface temperature, relative humidity,
277 wind speed, and surface O₃ concentrations to observations. The model reasonably
278 reproduces the spatial pattern of higher near-surface temperature in Southeast and
279 Northwest and lower temperature over the Tibetan Plateau (Figure 1a). On the national
280 scale, the near-surface temperature is underestimated with a mean bias (MB) of 1.04 °C
281 but it shows a high correlation (R=0.96). Unlike temperature, simulated relative
282 humidity is overestimated with a MB of 5.04 % but a high R of 0.93 (Figure 1b). Due
283 to the modeling biases in the topographic effects, simulated wind speed is overestimated

284 by more than 1.06 m s^{-1} on the national scale (Figure 1c). Such overestimation was also
285 reported in other studies using WRF models (Hu et al., 2016, Liu et al., 2020, Zhu et
286 al., 2022).

287 Comparisons with the measurements from air quality sites show that the simulated
288 O_3 deviates from the observed mean concentrations by $5.42 \mu\text{g m}^{-3}$ with a spatial R of
289 0.68. The model reasonably captures the hotspots over North China Plain though with
290 some overestimations, potentially attributed to uncertain emissions and coarse model
291 resolutions. Such elevated bias in summer O_3 is a common issue for both global and
292 regional models over Asia. For example, Zhu et al. (2022) reported the overestimated
293 summer average ozone concentration by $13.82 \mu\text{g m}^{-3}$ in China. Liu et al. (2020)
294 reached positive biases ranging from $3.7 \mu\text{g m}^{-3}$ to $13.32 \mu\text{g m}^{-3}$ using the WRF-CMAQ
295 model. Overall, the WRF-Chem model shows reasonable performance in the simulation
296 of surface meteorology and O_3 concentrations in China.

297

298 **3.2 Offline O_3 damage**

299 We compared the offline O_3 damage to photosynthesis between sunlit (PSNSUN)
300 and shaded (PSNSHA) leaves during the summer. The S2007 scheme is dependent on
301 instantaneous O_3 uptake, which peaks in July when both O_3 concentrations and stomatal
302 conductance are high (Figures S1 and S2). For the same O_3 pollution level, the damages
303 are much higher for the sunlit leaves (Figures 2a-2b) than that for the shaded leaves
304 (Figures 2d-2e), because of the higher stomatal conductance linked with the more active
305 photosynthesis for the sunlit leaves. In contrast, the L2013 scheme depends on the
306 accumulated O_3 flux and assumes constant damages for some PFTs (Table 2), resulting
307 in reductions of photosynthesis even at low O_3 concentrations. The O_3 damage to
308 photosynthesis of sunlit and shaded leaves increases month by month, reaching a
309 maximum in August (Figures S1 and S2). We found limited differences in the O_3
310 damages between sunlit (Figure 2c) and shaded (Figure 2f) leaves with L2013 scheme.
311 Observations have reported that surface O_3 has limited impacts on the shaded leaves
312 (Wan et al., 2014), consistent with the results simulated by the S2007 scheme.

313 Figure 3 shows the effect of O₃ damage to stomatal resistance of sunlit (RSSUN)
314 and shaded (RSSHA) leaves. Overall, the spatial pattern of the changes in stomatal
315 resistance is consistent with those of photosynthesis (Figure 2) but with opposite signs.
316 Both RSSUN and RSSHA are enhanced by O₃ damage so as to prevent more O₃ uptake.
317 For S2007 scheme, RSSUN with high and low sensitivities respectively increases by
318 13.43% (Figure 3a) and 8.35% (Figure 3b), higher than the rates of 4.71% (Figure 3d)
319 and 2.97% (Figure 3e) for RSSHA. These ratios are inversely connected to the changes
320 of photosynthesis (Figure 2), suggesting the full coupling of damages between leaf
321 photosynthesis and stomatal conductance. For L2013 scheme, predicted changes in
322 RSSUN (Figure 3c) and RSSHA (Figure 3f) are very similar with the magnitude of
323 25.3%-26.3%. These changes are higher than the loss of photosynthesis (Figures 2c and
324 2f), suggesting the decoupling of O₃ damages to leaf photosynthesis and stomatal
325 conductance as revealed by the L2013 scheme.

326 We further assessed the O₃ damage to GPP and transpiration (TR). For S2007
327 scheme, O₃ causes damages to national average GPP and TR approximately by 5.5%
328 with low sensitivity (Figures 4b and 4e) and 8.4% with high sensitivity (Figures 4a and
329 4d) compared to the CTRL simulation. The model predicts high GPP damages over
330 North China Plain and moderate damages in the southeastern and northeastern regions.
331 In the northwest, GPP damage is very limited due to the low relative humidity (Figure
332 1b) that constrains the stomatal uptake. For L2013 scheme, TR shows uniform
333 reductions exceeding -25% in most regions of China except for the northwest (Figure
334 4f), though O₃ concentrations show distinct spatial gradient (Figure 1d). The changes
335 of GPP are similar to that of TR but with lower inhibitions (Figure 4c). On average, the
336 GPP reduction with the L2013 scheme is 2.5-3.9 times of that predicted with the S2007
337 scheme. The most significant differences are located in Tibetan Plateau with limited
338 damages in S2007 but strong inhibitions of both GPP and TR in L2013. The low
339 temperature (Figure 1a) and O₃ concentrations (Figure 1d) jointly constrain O₃ stomatal
340 uptake (Figure S3), leading to low O₃ damages over Tibetan Plateau with the S2007
341 scheme. However, the L2013 scheme applies $b_p=0.8021$ for grassland (Table 2),

342 suggesting strong baseline damages up to 20% even with CUO=0 over Tibetan Plateau
343 where the grassland dominates (Figure S4).

344

345 **3.3 The O₃-vegetation feedback to surface energy and meteorology**

346 The O₃ vegetation damage causes contrasting responses in surface sensible heat
347 (SH) and LH (Figure 5). For S2007 scheme, the SH fluxes on average increase by 3.17
348 W m⁻² (8.85%) with low sensitivity (Figure 5b) and 5.99 W m⁻² (16.22%) with high
349 sensitivity (Figure 5a). The maximum enhancement is located in southern China, where
350 the increased stomatal resistance (Figure 3a) reduces transpiration and the consequent
351 heat dissipation. Meanwhile, LH fluxes decrease by 3.26 W m⁻² (5.58%) with low
352 sensitivity (Figure 5e) and 6.43 W m⁻² (15.29%) with high sensitivity (Figure 5d),
353 following the reductions in transpiration (Figures 4d and 4e). We found similar changes
354 in surface energy by O₃-vegetation coupling between the S2007 and L2013 schemes.
355 The SH shows the same hotspots over southern China with national average increase
356 of 12.85% (Figure 5c), which is within the range of 8.85% to 16.22% predicted by the
357 S2007 scheme. The LH largely decreases in central and northern China with the mean
358 reduction of 17.4% (Figure 5f), close to the magnitude of 15.29% predicted with the
359 S2007 scheme using the high O₃ sensitivity (Figure 5d). Although the offline damages
360 to GPP and TR are much larger with the L2013 than S2007 (Figure 4), their feedback
361 to surface energy shows consistent spatial pattern and magnitude (Figure 5), likely
362 because the O₃ inhibition in S2007 has the same diurnal cycle with energy fluxes while
363 the L2013 scheme shows almost constant inhibitions throughout the day (Figure S5).
364 The zero or near-zero slope parameters (a_p and a_c) in the L2013 scheme (Table 2) lead
365 to insensitive responses of photosynthesis and stomatal conductance to the variations
366 of CUO. As a result, there were very limited diurnal variations in O₃ damage with the
367 L2013 scheme. However, the strong nighttime damages in L2013 have limited
368 contributions to the changes of surface energy, which usually peaks at the daytime.

369 The O₃-induced damages to stomatal conductance weaken plant transpiration and
370 thus slow down the heat dissipation at the surface, leading to the higher temperature but

371 lower RH in China (Figure 6). On the national scale, temperature increases by 0.5 °C
372 due to O₃ vegetation damage with the high sensitivity (Figure 6a) and 0.23 °C with the
373 low sensitivity (Figure 6b) predicted using the S2007 scheme. A similar warming is
374 predicted with the L2013 scheme except that temperature shows moderate enhancement
375 over Tibetan Plateau (Figure 6c). The average RH decreases by 3.68% with the high O₃
376 sensitivity (Figure 6d) and 2.22% with the low sensitivity (Figure 6e) in response to the
377 suppressed plant transpiration. A stronger RH reduction of -3.85% is achieved with the
378 L2013 scheme, which predicts the maximum RH reductions in the North (Figure 6f).

379

380 **3.4 The O₃-vegetation feedback to air quality**

381 The O₃-induced inhibition on stomatal resistance leads to a significant increase in
382 surface O₃ concentrations, particularly in eastern China (Figures 7a-7c). The main cause
383 of such feedback is the reduction in O₃ dry deposition, which exacerbates the O₃
384 pollution in China. For S2007 scheme, this positive feedback can reach up to 15 μg m⁻³
385 ³ with high sensitivity (Figure 7a) and 8 μg m⁻³ with low sensitivity (Figure 7b) over
386 North China Plain. On the national scale, surface O₃ enhances 4.40 μg m⁻³ (5.08 %)
387 with high O₃ sensitivity and 2.62 μg m⁻³ (3.04%) with low O₃ sensitivity through the
388 coupling to vegetation. For L2013 scheme, the changes of O₃ concentration (Figure 7c)
389 are comparable to that of the S2007 scheme with high sensitivity (Figure 7a), except
390 that the O₃ enhancement is stronger in the Southeast but weaker in the Northeast.

391 The O₃-vegetation coupling also increases surface isoprene emissions. For S2007
392 scheme, isoprene emissions increase by 6.13% with high sensitivity (Figure 7d) and
393 3.43% with low sensitivity (Figure 7e), with regional hotspots in North China Plain,
394 northeastern and southern regions. The predictions using L2013 scheme (Figure 7f)
395 show very similar patterns and magnitude of isoprene changes to the S2007 scheme
396 with high sensitivity. Such enhancement in isoprene emissions is related to the
397 additional surface warming by O₃-vegetation interactions (Figures 6a-6c). In turn, the
398 increased isoprene emissions contribute to the deterioration of O₃ pollution in China.

399

400 **4. Conclusions and discussion**

401 In this study, we explored the feedback of O₃-vegetation coupling to surface
402 meteorology and air quality in China using two O₃ damage schemes embedded in a
403 regional meteorology-chemistry coupled model. The two schemes predicted distinct
404 spatial patterns with much larger magnitude of GPP loss in the L2013 scheme than that
405 in the S2007 scheme. We further distinguished the leaf responses with different
406 illuminations. For the S2007 scheme, the damages to photosynthesis of sunlit leaves
407 are ~2.6 times of that to shaded leaves. However, for the L2013 scheme, limited
408 differences are found between the sunlit and shaded leaves. The damages to leaf
409 photosynthesis increase stomatal resistance, leading to the reductions of transpiration
410 but enhancement of sensible heat due to the less efficient heat dissipation. These
411 changes in surface energy and water fluxes feed back to increase surface temperature
412 but decrease relative humidity. Although the L2013 scheme predicts much stronger
413 offline damages, the feedback causes very similar pattern and magnitude in surface
414 warming as the S2007 scheme. Consequently, surface O₃ increases due to the stomatal
415 closure and isoprene emissions enhance due to the anomalous warming.

416 Our predicted O₃ damage to GPP was within the range of -4% to -40% as estimated
417 in previous studies using different models and/or parameterizations over China (Ren et
418 al., 2011; Lombardozzi et al., 2015; Yue et al., 2015; Sadiq et al., 2017; Xie et al., 2019;
419 Zhu et al., 2022; Jin et al., 2023). Such a wide span revealed the large uncertainties in
420 the estimate of O₃ impacts on ecosystem functions. In this study, we employed two
421 schemes and compared their differences. With the S2007 scheme, we predicted GPP
422 reductions of -5.5% to -8.5% in China. This is similar to the range of -4% to -10%
423 estimated by Yue et al. (2015) using the same O₃ damage scheme. However, it is lower
424 than the estimate of -12.1% predicted by Xie et al. (2019), likely due to the slight
425 overestimation of surface O₃ in the latter study. With the L2013 scheme, we predicted
426 much larger GPP reductions of -21.4%. However, such value was still lower than the -
427 28.9% in Jin et al. (2023) and -20% to -40% in Zhu et al. (2022) using the same L2013
428 scheme embedded in WRF-Chem model, though all studies showed similar spatial

429 patterns in the GPP reductions. Such differences were likely attributed to the varied
430 model configuration as we ran the model from May while the other studies started from
431 the beginning of years. The longer time for the accumulation of O₃ stomatal uptake in
432 other studies might result in higher damages than our estimates with the L2013 scheme.

433 The O₃-vegetation coupling caused strong feedback to surface meteorology and
434 air quality. Our simulations with either scheme revealed that surface SH increases by
435 2-28 W m⁻² and LH decreases by 4-32 W m⁻² over eastern China, consistent with the
436 estimates of 5-30 W m⁻² by Zhu et al. (2022) using WRF-Chem model with the L2013
437 scheme. Consequently, surface air temperature on average increases by 0.23-0.51°C
438 while relative humidity decreases by 2.2-3.8%, similar to the warming of 0.2-0.8°C and
439 RH reduction of 3% as predicted by Zhu et al. (2022). However, these changes in
440 surface energy flux and meteorology are much higher than that in Jin et al. (2023),
441 likely because the latter focuses on the perturbations averaged throughout the year
442 instead of summer period as in this study and Zhu et al. (2022). We further predicted
443 that O₃ vegetation damage increased surface O₃ by 1.0-3.33 μg m⁻³ in China, similar
444 to the 2.35-4.11 μg m⁻³ estimated for eastern China using a global model (Gong et al.,
445 2020). Regionally, the O₃ enhancement reached as high as 7.84-14.70 μg m⁻³ in North
446 China Plain, consistent with the maximum value of 11.76 μg m⁻³ over the same domain
447 predicted by Zhu et al. (2022). However, limited feedback to surface O₃ was predicted
448 in Jin et al. (2023), mainly because the decreased dry deposition had comparable but
449 opposite effects to the decreased isoprene emissions due to the reductions of LAI. Such
450 discrepancy was likely caused by the stronger O₃ inhibition in Jin et al. (2023) following
451 the longer period of O₃ accumulation, consequently exacerbating the negative impacts
452 of LAI reductions on O₃ production.

453 There were some limitations in our parameterizations and simulations. First, we
454 predicted increases of isoprene emissions in eastern China mainly due to the increased
455 leaf temperature, which is in line with previous studies (Sadiq et al., 2017; Zhu et al.,
456 2022). However, isoprene production is coupled to photosynthesis. There are empirical
457 evidences showing that high dose of O₃ exposure reduces isoprene emissions when O₃

458 exposure is prolonged enough to suppress photosynthesis (Bellucci et al., 2023).
459 Inclusion of such negative feedback might alleviate the O₃-induced enhancement in
460 isoprene emissions. Second, the WRF-Chem model slightly overestimated summer O₃
461 concentrations, which could exacerbate the damages to stomatal conductance and the
462 subsequent feedback. Third, the S2007 scheme employed the coupled responses in
463 photosynthesis and stomatal conductance to O₃ vegetation damage. However, some
464 observations revealed that stomatal response is slow under long-term O₃ exposure,
465 resulting in loss of stomatal function and decoupling from photosynthesis (Calatayud
466 et al., 2007; Lombardozzi et al., 2012). The L2013 scheme considered the decoupling
467 between photosynthesis and stomatal conductance. However, this scheme shows no
468 significant different changes for sunlit and shaded leaves. In addition, the calculation
469 of CUO heavily relied on the O₃ threshold and accumulation period, leading to varied
470 responses among different studies using the same scheme. Furthermore, the slopes of
471 O₃ sensitivity in L2013 scheme were set to zero for some PFTs, leading to constant
472 damages independent of CUO. Fourth, the current knowledge of the O₃ effects on
473 stomatal conductance was primarily derived from leaf-level measurements (Matyssek
474 et al., 2008), which were much fewer compared to that for photosynthesis. The limited
475 data availability and lack of inter-PFT responses constrain the development of empirical
476 parameterizations.

477 Despite these limitations, our study provided the first comparison of different
478 parameterizations in simulating O₃-vegetation interactions. We found similar feedbacks
479 to surface energy and meteorology though the two schemes showed varied magnitude
480 and distribution in the offline responses of GPP and stomatal conductance to surface
481 O₃. The main cause of such inconsistency lied in the low feedback of damages in L2013
482 with some unrealistic inhibitions of ecosystem functions at night and over the regions
483 with low O₃ level. Such similarity provides a solid foundation for the exploration of
484 O₃-vegetation coupling using different schemes. The positive feedback of O₃ vegetation
485 damage to surface air temperature and O₃ concentrations posed emerging but ignored
486 threats to both climate change and air quality in China.

487

488 **Data availability.** The observed hourly O₃ concentrations were obtained from Chinese
489 National Environmental Monitoring Center (CNEMC, <http://websearch.mep.gov.cn/>).
490 The observed meteorological data were obtained from the National Meteorological
491 Information Center of China Meteorological Administration (CMA Meteorological
492 Data Centre, 2022, <http://data.cma.cn/data/detail/dataCode/A.0012.0001.html>). The
493 MEIC and MIX emission inventory are available at
494 http://meicmodel.org.cn/?page_id=560 and http://meicmodel.org.cn/?page_id=89.

495

496 **Author contributions.** XY conceived the study. XY and JC designed the research and
497 carried out the simulations. JC completed data analysis and the first draft. MM provided
498 useful comments on the paper. XY reviewed and edited the manuscript.

499

500 **Competing interests.** The authors declare that they have no conflict of interest.

501

502 **Acknowledgements.** The authors are grateful to three anonymous reviewers for their
503 constructive comments that have improved this study.

504

505 **Financial support.** This study was jointly funded by the National Key Research and
506 Development Program of China (grant no. 2023YFF0805403), National Natural
507 Science Foundation of China (grant no. 42293323), and Jiangsu Funding Program for
508 Excellent Postdoctoral Talent (grant no. 2023ZB737).

509

510 **References**

511 Ainsworth, E. A., Yendrek, C. R., Sitch, S., Collins, W. J., and Emberson, L. D.: The
512 effects of tropospheric ozone on net primary productivity and implications for
513 climate change, *Annu. Rev. Plant Biol.*, 63, 637–661,
514 <https://doi.org/10.1146/annurevarplant-042110-103829>, 2012.

515 Ball, J. T., Woodrow, I. E., and Berry, J. A.: A model predicting stomatal conductance
516 and its contribution to the control of photosynthesis under different environmental

517 conditions, *Prog. Photosynthesis*, Springer, Dordrecht, 4, 221–224, 1987.

518 Bellucci, M., Locato, V., Sharkey, T. D., Gara D. and Loreto, F.: Isoprene emission by
519 plants in polluted environments, *J PLANT INTERACT.*, 18:1, 2266463,
520 <https://doi.org/10.1080/17429145.2023.2266463>, 2023

521 Calatayud, V., Cerveró, J., and Sanz, M. J.: Foliar, physiological and growth responses
522 of four maple species exposed to ozone, *Water Air Soil Pollut.*, 185, 239–254,
523 <https://doi.org/10.1007/s11270-007-9446-5>, 2007.

524 Chou, M.-D. and Suarez, M.J.: An Efficient Thermal Infrared Radiation
525 Parameterization for Use in General Circulation Models. Technical Report, 85p.
526 1994.

527 Dickinson, R. E.: Land surface processes and climate – Surface albedos and energy
528 balance, *Adv. Geophys.*, 25, 305–353, [https://doi.org/10.1016/S0065-](https://doi.org/10.1016/S0065-2687(08)60176-4)
529 [2687\(08\)60176-4](https://doi.org/10.1016/S0065-2687(08)60176-4), 1983.

530 Emmons, L. K., Walters, S., Hess, P. G., Lamarque, J.-F., Pfister, G. G., Fillmore, D.,
531 Granier, C., Guenther, A., Kinnison, D., Laepple, T., Orlando, J., Tie, X., Tyndall,
532 G., Wiedinmyer, C., Baughcum, S. L., and Kloster, S.: Description and evaluation
533 of the Model for Ozone and Related chemical Tracers, version 4 (MOZART-4),
534 *Geosci. Model Dev.*, 3, 43–67, <https://doi.org/10.5194/gmd-3-43-2010>, 2010.

535 Farquhar, G. D., Caemmerer, S. V., and Berry, J. A.: A biochemical model of
536 photosynthetic CO₂ assimilation in leaves of C₃ species, *Planta*, 149, 78–90,
537 <https://doi.org/10.1007/bf00386231>, 1980.

538 Felzer, B., Kicklighter, D., Melillo, J., Wang, C., Zhuang, Q., and Prinn, R.: Effects of
539 ozone on net primary production and carbon sequestration in the conterminous
540 United States using a biogeochemistry model, *Tellus B*, 56, 230–248,
541 <https://doi.org/10.1111/j.1600-0889.2004.00097.x>, 2004.

542 Feng, Z., Hu, E., Wang, X., Jiang, L., and Liu, X.: Ground-level O₃ pollution and its
543 impacts on food crops in China: A review, *Environ. Pollut.*, 199, 42–48,
544 <https://doi.org/10.1016/j.envpol.2015.01.016>, 2015.

545 Gong, C., Lei, Y., Ma, Y., Yue, X., and Liao, H.: Ozone– vegetation feedback through

546 dry deposition and isoprene emissions in a global chemistry–carbon–climate
547 model, *Atmos. Chem. Phys.*, 20, 3841–3857, [https://doi.org/10.5194/acp-203841-](https://doi.org/10.5194/acp-203841-2020)
548 2020, 2020.

549 Gong, C., Yue ,X., Liao, H., and Ma, Y.: A humidity-based exposure index representing
550 ozone damage effects on vegetation, *Environ. Res. Lett.*, 16, 044030,
551 <https://doi.org/10.1088/1748-9326/abecbb>, 2021.

552 Grell, G. A., McKeen, S., Michalakes, J., Bao, J.-W., Trainer, M., and Hsie, E.-Y.: Real-
553 time simultaneous prediction of air pollution and weather during the Houston 2000
554 Field Experiment, presented at the 4th Conference on Atmospheric Chemistry:
555 Atmospheric Chemistry and Texas Field Study, 13–17 January, American
556 Meteorological Society, Orlando, 2002.

557 Grell, G. A., Peckham, S. E., Schmitz, R., McKeen, S. A., Frost, G., Skamarock, W. C.,
558 and Eder, B.: Fully coupled “online” chem- istry within the WRF model. *Atmos.*
559 *Environ.*, 39, 6957–6975, <https://doi.org/10.1016/j.atmosenv.2005.04.027>, 2005.

560 Guenther, A., Karl, T., Harley, P., Wiedinmyer, C., Palmer, P. I., and Geron, C.:
561 Estimates of global terrestrial isoprene emissions using MEGAN (Model of
562 Emissions of Gases and Aerosols from Nature), *Atmos. Chem. Phys.*, 6, 3181–
563 3210, <https://doi.org/10.5194/acp-6-3181-2006>, 2006.

564 Hersbach, H., Bell, B., Berrisford, P., Hirahara, S., Horányi, A., Muñoz-Sabater, J.,
565 Nicolas, J., Peubey, C., Radu, R., Schepers, D., Simmons, A., Soci, C., Abdalla,
566 S., Abellan, X., Balsamo, G., Bechtold, P., Biavati, G., Bidlot, J., Bonavita, M., De
567 Chiara, G., Dahlgren, P., Dee, D., Diamantakis, M., Dragani, R., Flemming, J.,
568 Forbes, R., Fuentes, M., Geer, A., Haimberger, L., Healy, S., Hogan, R. J., Hólm,
569 E., Janisková, M., Keeley, S., Laloyaux, P., Lopez, P., Lupu, C., Radnoti, G., de
570 Rosnay, P., Rozum, I., Vamborg, F., Villaume, S., and Thépaut, J.-N.: The ERA5
571 global reanalysis, *Q. J. Roy. Meteor. Soc.*, 146, 1999–2049, 2020.

572 Hong, S.-Y., Noh, Y., and Dudhia, J.: A new vertical diffusion package with explicit
573 treatment of entrainment processes, *Mon. Weather Rev.*, 134, 2318–2341,
574 <https://doi.org/10.1175/MWR3199.1>, 2006.

575 Hu, J., Chen, J., Ying, Q., and Zhang, H.: One-year simulation of ozone and particulate
576 matter in China using WRF/CMAQ modeling system, *Atmos. Chem. Phys.*, 16,
577 10333–10350, <https://doi.org/10.5194/acp-16-10333-2016>, 2016.

578 Jin, Z., Yan, D., Zhang, Z., Li, M., Wang, T., Huang, X., Xie, M., Li S and Zhuang.:
579 Effects of elevated ozone exposure on regional meteorology and air quality in
580 China through ozone-vegetation coupling. *J. Geophys. Res.-Atmos.*, 128,
581 e2022JD038119. <https://doi.org/10.1029/2022JD038119>, 2023.

582 Li, J., Mahalov, A., and Hyde, P.: Simulating the impacts of chronic ozone exposure on
583 plant conductance and photosynthesis, and on the regional hydroclimate using
584 WRF/Chem, *Environ. Res. Lett.*, 11, 114017,
585 <https://doi.org/10.1088/17489326/11/11/114017>, 2016.

586 Li, P., Calatayud, V., Gao, F., Uddling, J., and Feng, Z. Z.: Differences in ozone
587 sensitivity among woody species are related to leaf morphology and antioxidant
588 levels, *Tree Physiol.*, 36, 1105– 1116, <https://doi.org/10.1093/treephys/tpw042>,
589 2016.

590 Li, P., Feng, Z., Catalayud, V., Yuan, X., Xu, Y., and Paoletti, E.: A meta-analysis on
591 growth, physiological, and biochemical responses of woody species to ground-
592 level ozone highlights the role of plant functional types, *Plant Cell Environ.*, 40,
593 2369–2380, <https://doi.org/10.1111/pce.13043>, 2017.

594 Liu, Y. and Wang, T.: Worsening urban ozone pollution in China from 2013 to 2017 –
595 Part 1: The complex and varying roles of meteorology, *Atmos. Chem. Phys.*, 20,
596 6305–6321, <https://doi.org/10.5194/acp-20-6305-2020>, 2020.

597 Lombardozzi, D., Levis, S., Bonan, G., and Sparks, J. P.: Predicting photosynthesis and
598 transpiration responses to ozone: decoupling modeled photosynthesis and stomatal
599 conductance, *Biogeosciences*, 9, 3113–3130, <https://doi.org/10.5194/bg-9-31132012>, 2012.

601 Lombardozzi, D., Sparks, J. P., and Bonan, G.: Integrating O₃ influences on terrestrial
602 processes: photosynthetic and stomatal response data available for regional and
603 global modeling, *Biogeosciences*, 10, 6815–6831, <https://doi.org/10.5194/bg-10-68152013>, 2013.

604 6815-2013, 2013.

605 Lombardozzi, D., Levis, S., Bonan, G., Hess, P. G., and Sparks, J. P.: The influence of
606 chronic ozone exposure on global carbon and water cycles, *J. Climate*, 28, 292–
607 305, <https://doi.org/10.1175/JCLI-D-14-00223.1>, 2015.

608 Matyssek, R., Sandermann, H., Wieser, G., Booker, F., Cieslik, S., Musselman, R., and
609 Ernst, D.: The challenge of making ozone risk assessment for forest trees more
610 mechanistic, *Environ. Pollut.*, 156, 567–582,
611 <https://doi.org/10.1016/j.envpol.2008.04.017>, 2008.

612 Mlawer, E. J., Taubman, S. J., Brown, P. D., Iacono, M. J., and Clough, S. A.: Radiative
613 transfer for inhomogeneous atmosphere: RRTM, a validated correlated-k model
614 for the longwave, *J. Geophys. Res-Atmos.*, 102(D14), 663–682,
615 <https://doi.org/10.1029/97JD00237>, 1997.

616 Monks, P. S., Archibald, A. T., Colette, A., Cooper, O., Coyle, M., Derwent, R., Fowler,
617 D., Granier, C., Law, K. S., Mills, G. E., Stevenson, D. S., Tarasova, O., Thouret,
618 V., von Schneidmesser, E., Sommariva, R., Wild, O., and Williams, M. L.:
619 Tropospheric ozone and its precursors from the urban to the global scale from air
620 quality to short-lived climate forcer, *Atmos. Chem. Phys.*, 15, 8889–8973,
621 <https://doi.org/10.5194/acp-15-8889-2015>, 2015.

622 Morrison, H., Thompson, G., and Tatarskii, V.: Impact of cloud microphysics on the
623 development of trailing stratiform precipitation in a simulated squall line:
624 comparison of one- and two-moment schemes, *Monthly Weather Review*, 137,
625 991–1007, <https://doi.org/10.1175/2008MWR2556.1>, 2009.

626 Niu, G. Y., Yang, Z. L., Mitchell, K. E., Chen, F., Ek, M. B., Barlage, M., Kumar, A.,
627 Manning, K., Niyogi, D., Rosero, E., Tewari, M., and Xia, Y.: The community
628 Noah land surface model with multiparameterization options (Noah-MP): 1.
629 Model description and evaluation with local-scale measurements, *J. Geophys.*
630 *Res-Atmos.*, 116, D12, <https://doi.org/10.1029/2010JD015139>, 2011.

631 Ren, W., Tian, H., Tao, B., Chappelka, A., Sun, G., Lu, C., Liu, M., Chen, G., and Xu,
632 X.: Impacts of tropospheric ozone and climate change on net primary productivity

633 and net carbon exchange of China's forest ecosystems, *Glob. Ecol. Biogeogr.*, 20,
634 391–406, <https://doi.org/10.1111/j.1466-8238.2010.00606.x>, 2011.

635 Sadiq, M., Tai, A. P. K., Lombardozzi, D., and Val Martin, M.: Effects of ozone–
636 vegetation coupling on surface ozone air quality via biogeochemical and
637 meteorological feedbacks, *Atmos. Chem. Phys.*, 17, 3055–3066,
638 <https://doi.org/10.5194/acp-17-3055-2017>, 2017.

639 Sitch, S., Cox, P. M., Collins, W. J., and Huntingford, C.: Indirect radiative forcing of
640 climate change through ozone effects on the land-carbon sink, *Nature*, 448, 791–
641 794, <https://doi.org/10.1038/nature06059>, 2007.

642 Skamarock W C and Klemp J B. A time-split nonhydrostatic atmospheric model for
643 weather research and forecasting applications. *J. Comput. Phys.*, 227(7): 3465–
644 3485, <https://doi.org/10.1016/j.jcp.2007.01.037>, 2008.

645 Su, B., Zhou, M., Xu, H., Zhang, X., Li, Y., Su, H., and Xiang B.: Photosynthesis and
646 biochemical responses to elevated O₃ in *Plantago major* and *Sonchus oleraceus*
647 growing in a lowland habitat of northern China, *J. Environ. SCI.*, 53(3): 113-121,
648 <https://doi.org/10.1016/j.jes.2016.05.011>, 2017.

649 Tie, X. X., Madronich, S., Walters, S., Zhang, R. Y., Rasch, P., and Collins, W.: Effect
650 of clouds on photolysis and oxidants in the troposphere, *J. Geophys. Res.-Atmos.*,
651 108, 4642, <https://doi.org/10.1029/2003jd003659>, 2003.

652 Wan, W., Manning, WJ., Wang, X., Zhang, H., Sun, X., and Zhang, Q.: Ozone and
653 ozone injury on plants in and around Beijing, China, *Environ Pollut.*, 191: 215–
654 222, <https://doi.org/10.1016/j.envpol.2014.02.035>, 2014

655 Wilkinson, S., Clephan, A. L., and Davies, W. J.: Rapid Low Temperature-Induced
656 Stomatal Closure Occurs in Cold-Tolerant *Commelina Communis* Leaves But Not
657 in Cold-Sensitive Tobacco Leaves, via a Mechanism That Involves Apoplastic
658 Calcium But Not Abscisic Acid. *Plant Physiol.*, 126, 1566–1578.
659 <https://doi.org/10.1104/pp.126.4.1566>, 2001.

660 Wittig, V. E., Ainsworth, E. A., and Long, S. P.: To what extent do current and projected
661 increases in surface ozone affect photosynthesis and stomatal conductance of trees?

662 A metaanalytic review of the last 3 decades of experiments, *Plant Cell Environ.*,
663 30, 1150–1162, <https://doi.org/10.1111/j.13653040.2007.01717.x>, 2007.

664 Xie, X., Wang, T., Yue, X., Li, S., Zhuang, B., Wang, M., and Yang, X.: Numerical
665 modeling of ozone damage to plants and its effects on atmospheric CO₂ in China,
666 *Atmos. Environ.*, 217, 116970, <https://doi.org/10.1016/j.atmosenv.2019.116970>,
667 2019.

668 Yue, X. and Unger, N.: Ozone vegetation damage effects on gross primary productivity
669 in the United States, *Atmos. Chem. Phys.*, 14, 9137–9153,
670 <https://doi.org/10.5194/acp-14-9137-2014>, 2014.

671 Yue, X. and Unger, N.: The Yale Interactive terrestrial Biosphere model version 1.0:
672 description, evaluation and implementation into NASA GISS ModelE2, *Geosci.*
673 *Model Dev.*, 8, 2399–2417, <https://doi.org/10.5194/gmd-8-2399-2015>, 2015.

674 Zaveri, R. A., and Peters, L. K.: A new lumped structure photochemical mechanism for
675 large-scale applications, *J Geophys Res-Atmos*, 104, 30387-30415, 1999.

676 Zaveri, R. A., Easter, R. C., Fast, J. D., and Peters, L. K.: Model for simulating aerosol
677 interactions and chemistry (MOSAIC), *J. Geophys. Res-Atmos.*, 113, D13204,
678 <https://doi.org/10.1029/2007JD008782>, 2008.

679 Zhou, S. S., Tai, A. P. K., Sun, S., Sadiq, M., Heald, C. L., and Geddes, J. A.: Coupling
680 between surface ozone and leaf area index in a chemical transport model: strength
681 of feedback and implications for ozone air quality and vegetation health, *Atmos.*
682 *Chem. Phys.*, 18, 14133–14148, <https://doi.org/10.5194/acp-18-14133-2018>, 2018.

683 Zhu, J., Tai, A. P. K., and Yim, S. H. L.: Effects of ozone-vegetation interactions on
684 meteorology and air quality in China using a two-way coupled land-atmosphere
685 model, *Atmos. Chem. Phys.*, 22, 765-782, [https://doi.org/10.5194/acp-22-765-](https://doi.org/10.5194/acp-22-765-2022)
686 2022, 2022.

687

688 **Tables**689 **Table 1.** Parameters used for S2007 O₃ damage scheme ^a.

PFTs ^b	$a_{PFT}(\text{nmol}^{-1} \text{m}^2 \text{s})$ ^c	$\gamma_{PFT}(\text{nmol m}^{-2} \text{s}^{-1})$
EBF	0.075, 0.02	1.6
NF	0.075, 0.02	1.6
DBF	0.15, 0.04	1.6
SHR	0.1, 0.03	1.6
GRA	1.4, 0.25	5
CRO	1.4, 0.25	5

690 ^a The data source is Sitch et al. (2007).691 ^b The plant functional types (PFTs) include evergreen broadleaf forest (EBF), needleleaf
692 forest (NF), deciduous broadleaf forest (DBF), shrubland (SHR), grassland (GRA), and
693 cropland (CRO).694 ^c The first number is for high sensitivity and the second is for low sensitivity.

695

696

697

Table 2. Slopes and intercepts used for L2013 O₃ damage scheme ^a.

PFTs	a_p (mmol m ⁻²)	b_p	a_c (mmol m ⁻²)	b_c
EBF	0	0.8752	0	0.9125
NF	0	0.839	0.0048	0.7823
DBF	0	0.8752	0	0.9125
SHR	0	0.8752	0	0.9125
GRA	-0.0009	0.8021	0	0.7511
CRO	-0.0009	0.8021	0	0.7511

698

^a The data source is Lombardozzi et al. (2015). Due to the data limit, we apply the same

699

sensitivity parameters for EBF, DBF, and SHR.

700

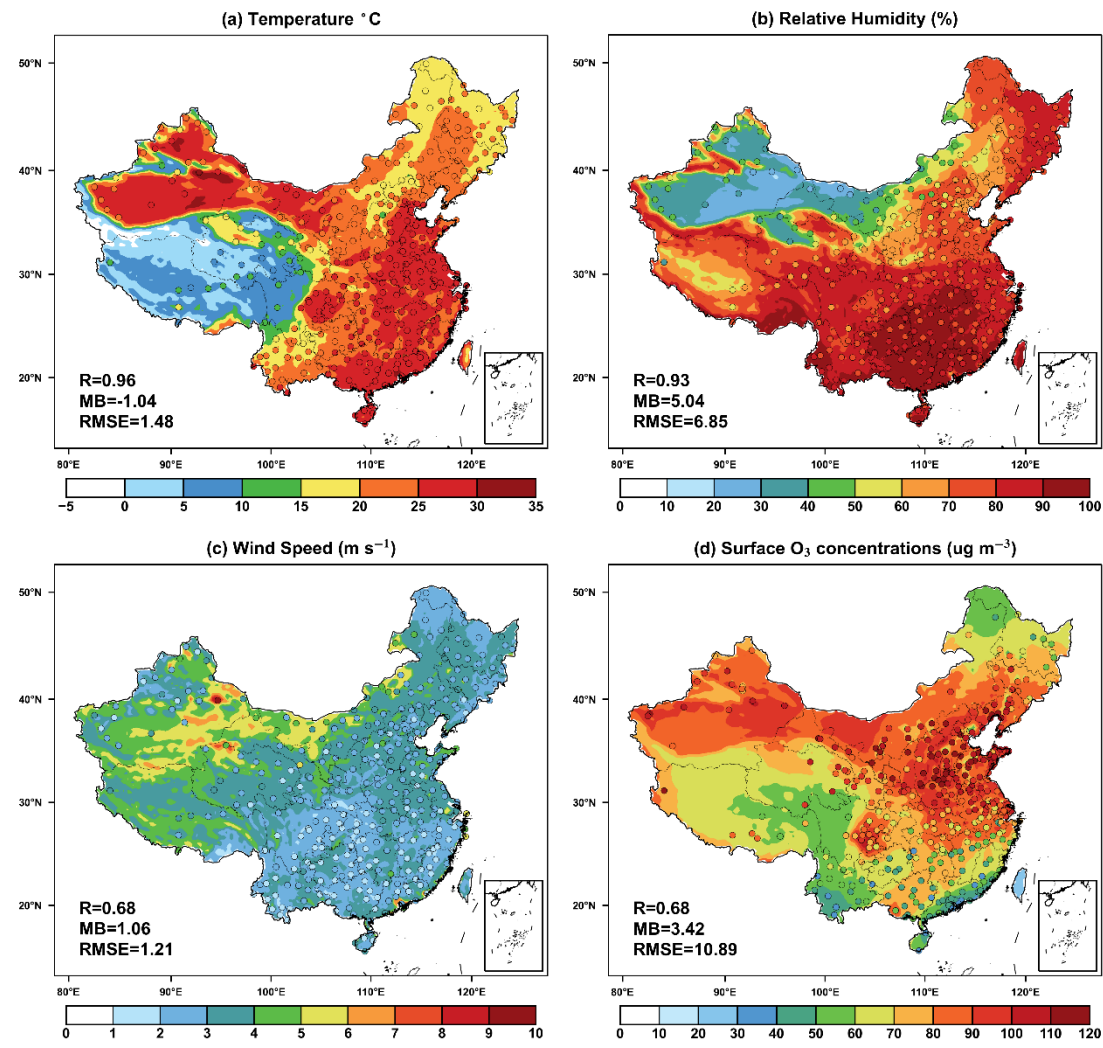
701

Table 3. Summary of simulation experiments

Name	O ₃ damage to vegetable	Scheme
CRTL	-	-
Offline_SH07	High	Sitch et al. (2007)
Offline_SL07	Low	Sitch et al. (2007)
Offline_L13	-	Lombardozzi et al. (2013)
Online_SH07	High	Sitch et al. (2007)
Online_SL07	Low	Sitch et al. (2007)
Online_L13	-	Lombardozzi et al. (2013)

702

703



705

706

707

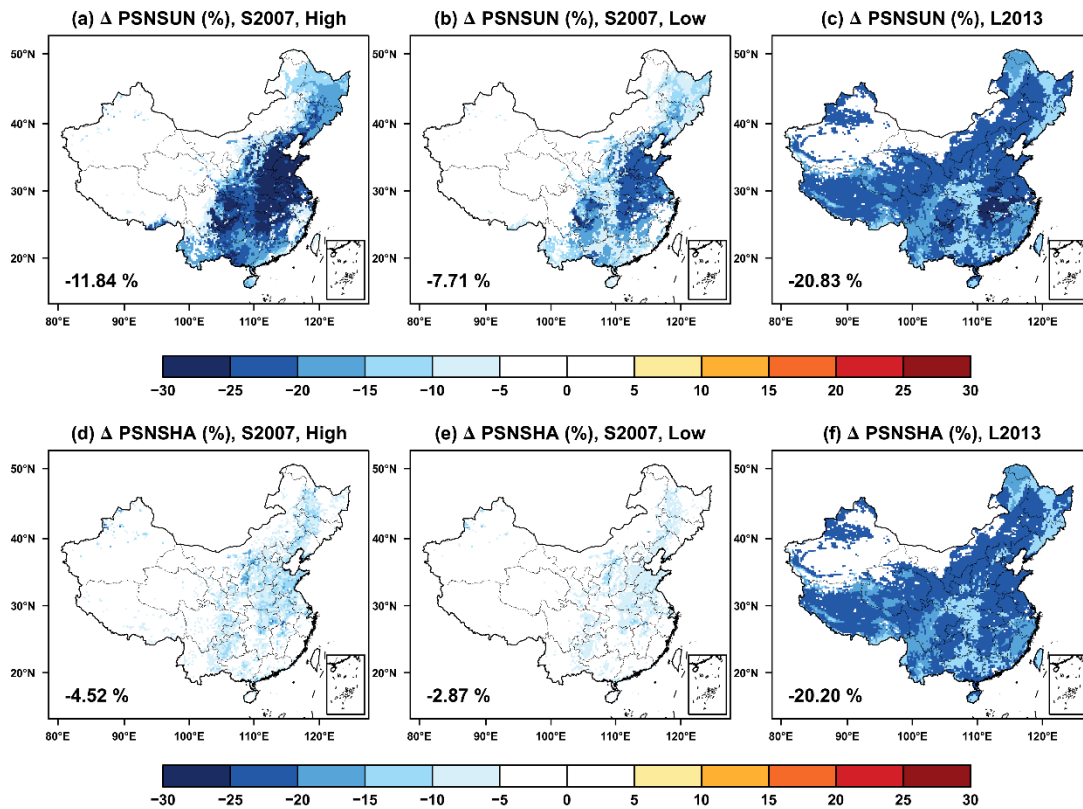
708 **Figure 1** Evaluations of simulated summer (June–August) daily (24-h average) (a)709 near-surface temperature, (b) relative humidity, (c) wind speed, and (d) surface O_3

710 concentrations in China. The dots represent the site-level observations. The correlation

711 coefficients (R), mean biases (MB), and root-mean-square error (RMSE) for the

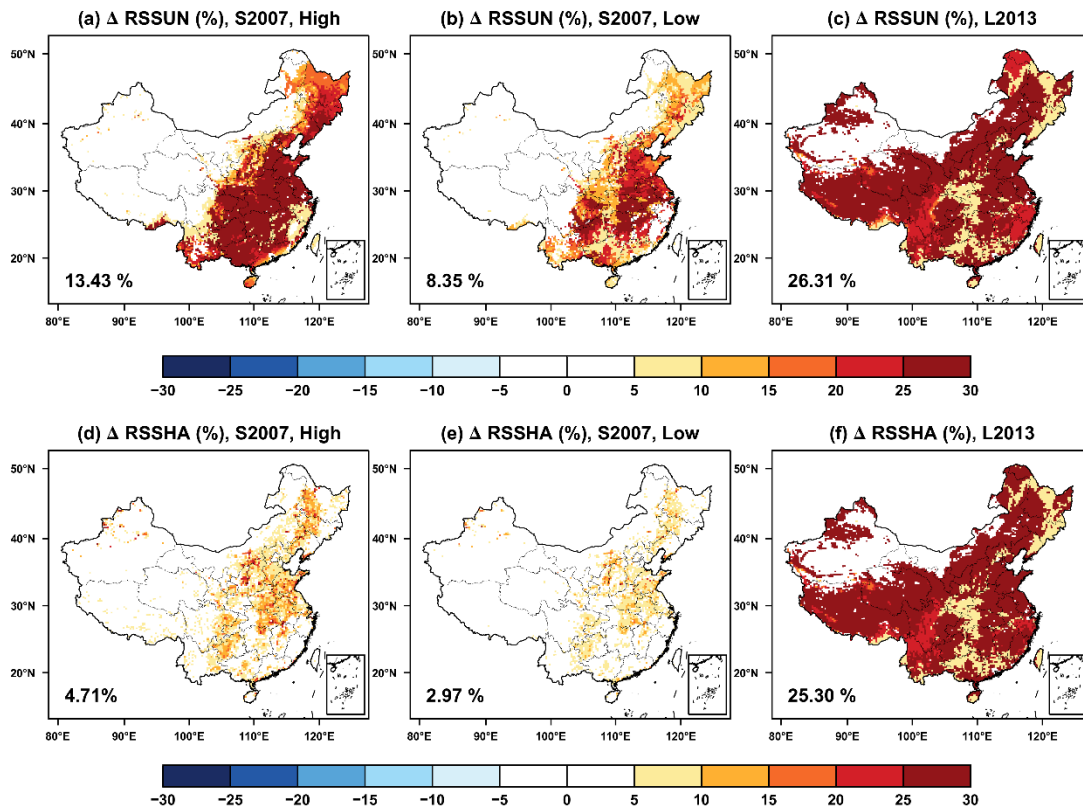
712 comparisons are shown in the lower left corner of each panel.

713



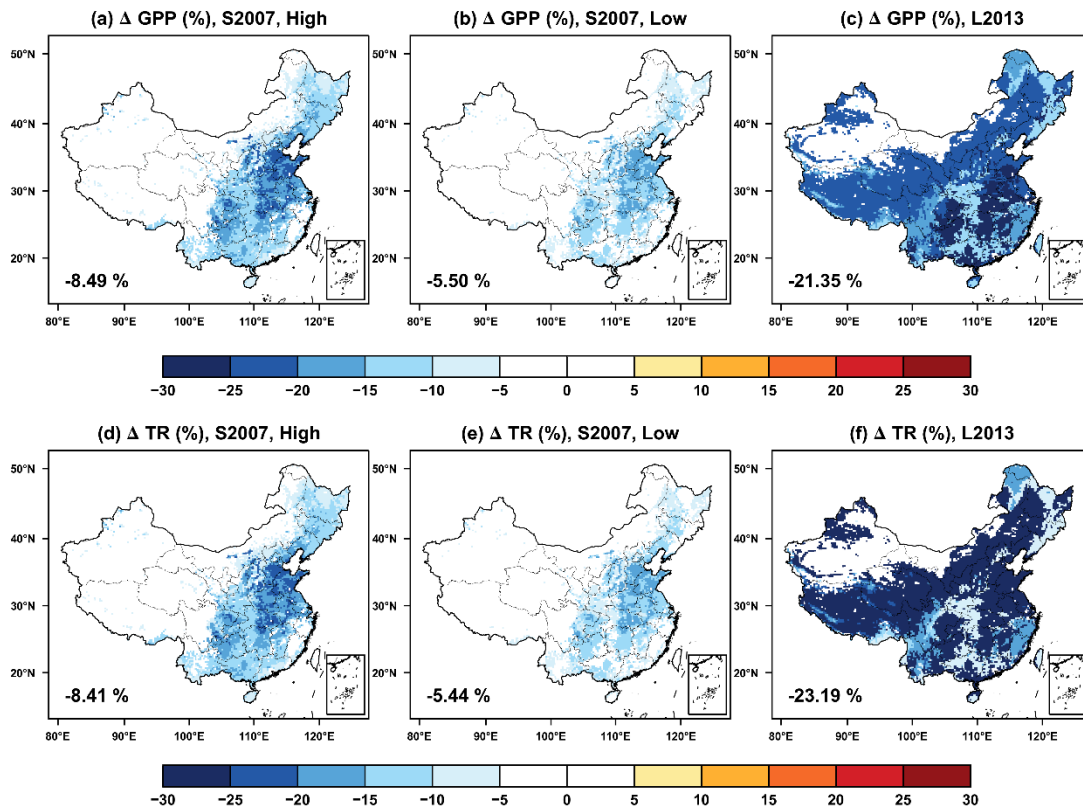
714
 715
 716
 717
 718
 719
 720

Figure 2 Offline O₃ damage (%) to the summertime photosynthesis of (a-c) sunlit and (d-f) shaded leaves predicted by the S2007 scheme with (a, d) high and (b, e) low sensitivities or the (c, f) L2013 scheme. The area-weighted percentage changes are shown in the lower left corner.



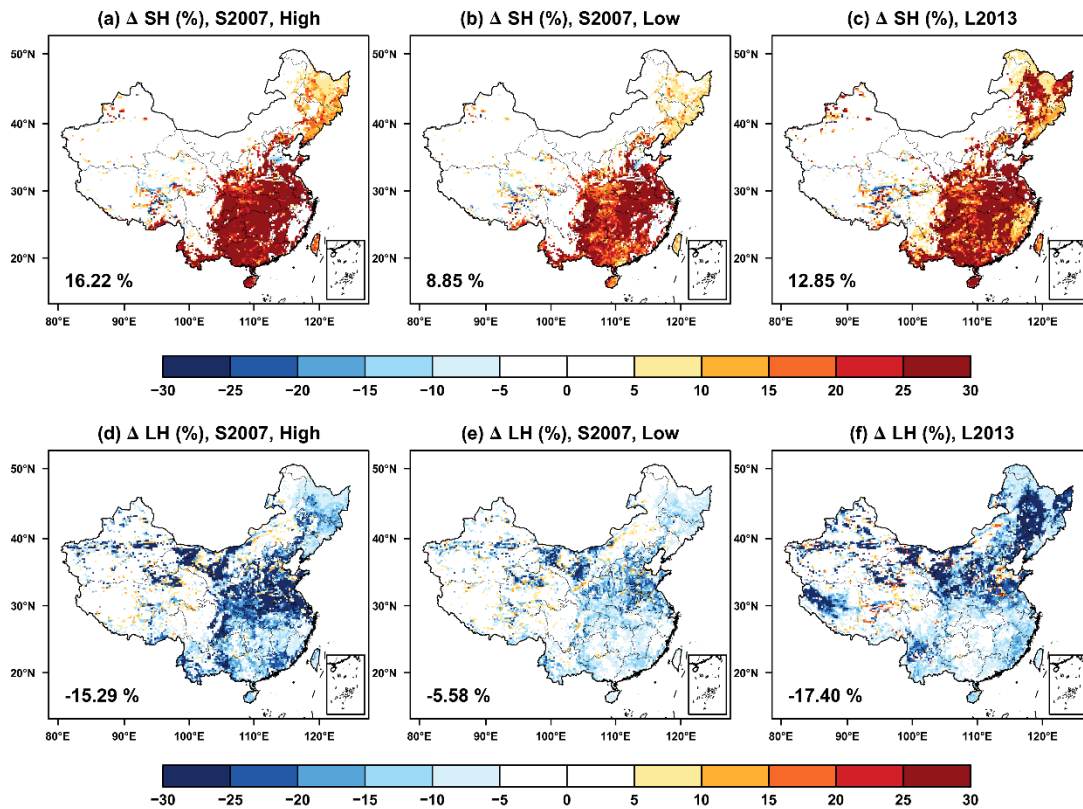
721
 722
 723
 724

Figure 3 The same as Figure 2 but for the changes in stomatal resistance.



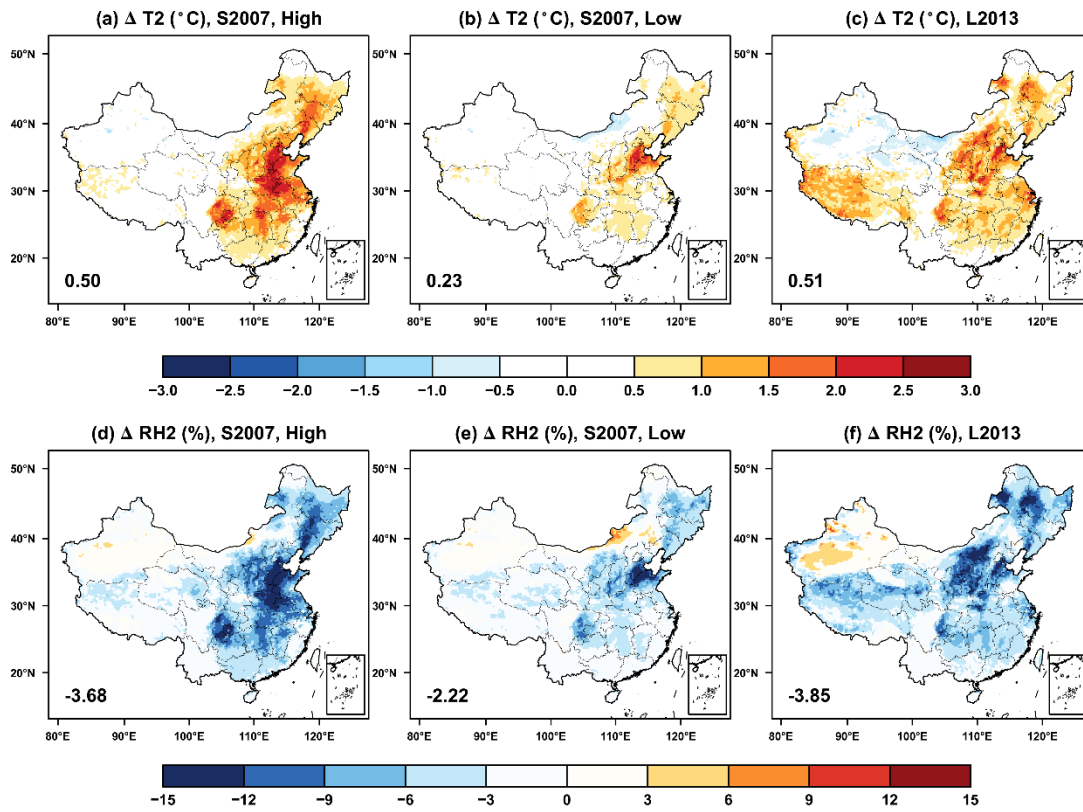
725
726
727
728
729
730
731

Figure 4 Offline O₃ damage (%) to the (a-c) gross primary productivity (GPP) and (d-f) transpiration rate (TR) predicted by the Sitch scheme with (a, d) high and (b,e) low sensitivities or the (c, f) Lombardozzi scheme. The area-weighted percentage changes are shown in the lower left corner.



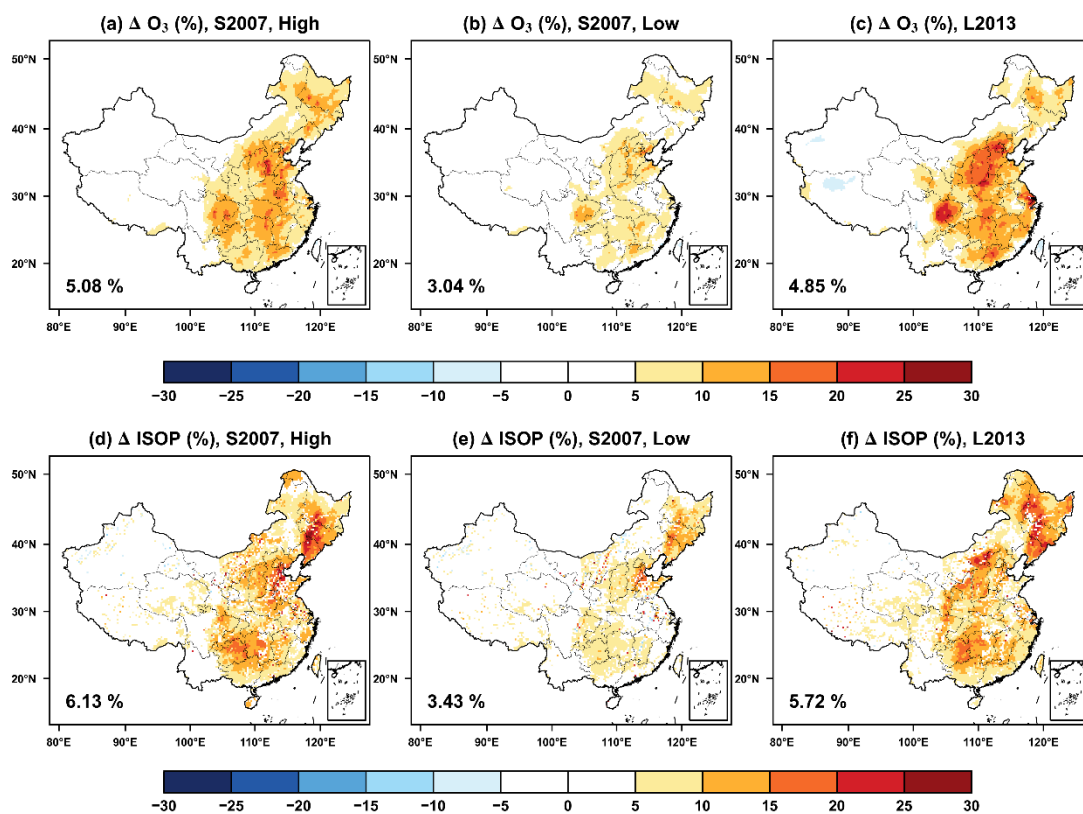
732
 733
 734
 735
 736
 737
 738
 739

Figure 5 The feedback of O₃-vegetation interaction to surface (a-c) sensible and (d-f) latent heat fluxes in the summer predicted by the S2007 scheme with (a, d) high and (b, e) low sensitivities or the (c, f) L2013 scheme. The relative changes are shown with area-weighted percentage changes indicated at the lower left corner.



740
 741
 742
 743
 744
 745

Figure 6 The same as Figure 5 but for changes in (top) air temperature and (bottom) relative humidity at 2 meters.



747

748

749 **Figure 7** The feedback of O₃-vegetation interaction to surface O₃ concentrations and
 750 isoprene emissions in the summer predicted by the S2007 scheme with (a, d) high and
 751 (b, e) low sensitivities or the (c, f) L2013 scheme. The area-weighted percentage
 752 changes are shown in the lower left corner.

753